The Astronomical Journal, 145:73 (7pp), 2013 March doi:10.1088/0004-6256/145/3/73

ON THE RADIO AND NEAR-INFRARED JET OF PKS 2155−304 AND ITS CLOSE ENVIRONMENT

E. Liuzzo[1], R. Falomo[2], A. Treves[3], C. Arcidiacono[4], E. Torresi[5], M. Uslenghi[6], J. Farinato[2], A. Moretti[2], R. Ragazzoni[2], E. Diolaiti[4], M. Lombini[4], R. Brast[7], R. Donaldson[8], J. Kolb[8], E. Marchetti[8], and S. Tordo[8]
[1] Istituto di Radioastronomia, INAF, Via Gobetti 101, I-40129 Bologna, Italy; liuzzo@ira.inaf.it
[2] Osservatorio Astronomico di Padova, INAF, vicolo dell'Osservatorio 5, I-35122 Padova, Italy
[3] INAF and INFN, Università dell'Insubria (Como), via Valleggio 11, I-22100 Como, Italy
[4] Osservatorio Astronomico di Bologna, INAF, Bologna, Via Ranzani 1, I-40127 Bologna, Italy
[5] INAF/IASF Bologna, Via Gobetti 101, I-40129 Bologna, Italy
[6] INAF/IASF Milano, Via E. Bassini 15, I-20133 Milano, Italy
[7] Dipartimento di Astronomia, Università di Bologna, Via Ranzani 1, I-40127 Bologna, Italy
[8] European Southern Observatory, Karl-Schwarschild-Str 2, D-85748 Garching bei München, Germany
Received 2012 November 1; accepted 2013 January 3; published 2013 February 11

ABSTRACT

PKS 2155−304 is one of the brightest BL Lac objects in the sky and a very well-studied target from radio to TeV bands. We report on high-resolution (∼0.″12) direct imaging of the field of PKS 2155−304 using adaptive optics near-IR (NIR) observations in the *J* and *Ks* bands obtained with the ESO Multi-Conjugate Adaptive Optics Demonstrator on the Very Large Telescope. These data are complemented with archival Very Large Array images at various frequencies to investigate the properties of the close environment of the source. We characterize the faint galaxies that form the poor group associated with the target. No radio emission is present for these galaxies, while an old radio jet at ∼20 kpc from the nucleus of PKS 2155−304 and a jet-like structure of ∼2 kpc (∼1″) in the eastern direction are revealed. No counterparts of these radio jets are found in the NIR or in archival *Chandra* observations.

Key words: BL Lacertae objects: individual (PKS 2155-304) – instrumentation: adaptive optics

Online-only material: color figures

1. INTRODUCTION

PKS 2155−304 ($V \sim 13$, $z = 0.116$) is one of the best studied BL Lac objects from radio to TeV bands (Urry et al. 1993, 1997; Aharonian et al. 2005, 2007, 2009; Foschini et al. 2007, 2008 and references therein). It is an archetypal X-ray-selected BL Lac object that is well known to be rapidly and strongly variable throughout the whole electromagnetic spectrum on diverse timescales (e.g., Aharonian et al. 2005; Marshall et al. 2001; Piner & Edwards 2004; Piner et al. 2008, 2010 and references therein). Many researchers have also found evidence of ultra-relativistic outflows (Aharonian et al. 2007; Foschini et al. 2007; Sakamoto et al. 2008).

At radio frequencies, the low-resolution (∼2″) Very Large Array (VLA) images presented by Ulvestad & Antonucci (1986) and Laurent-Muehleisen et al. (1993) show an extended (∼1′) halo around the core. At higher resolution (∼0.″6), VLA images reveal a knot at 10″ in the NW direction nearly 180° misaligned from the parsec-scale jet reported by Piner et al. (2010 and references therein). At the milliarcsecond scale, very long baseline interferometer (VLBI) maps have been presented by several authors (Ojha et al. 2004, 2010; Piner & Edwards 2004; Piner et al. 2008, 2010). The apparent speeds of jet components are also measured (e.g., Piner et al. 2010), and jet bending on parsec scales is found.

In the optical and near-IR (NIR) bands, PKS 2155−304 was observed with various instruments to study its host galaxy (Falomo et al. 1991; Kotilainen et al. 1998). It was found that the object is hosted by a luminous elliptical galaxy ($M_R = -24.4$ and $M_H = -26.8$) at a redshift of 0.116 (Falomo et al. 1993; Sbarufatti et al. 2006). The field around the object is moderately rich in galaxies. Spectroscopy of some of them shows that they are at the same redshift of the BL Lac source, indicating that its host galaxy is the dominant member of a group of galaxies. The closest companion galaxy is found 4.″6 (∼9.7 kpc) from the source (Falomo et al. 1991, 1993).

Curiously, while several BL Lac objects were imaged by *Hubble Space Telescope* (*HST*) cameras during various campaigns (see, e.g., Scarpa et al. 2000), PKS 2155−304 was never observed with *HST* and the best available high-resolution images in the optical band remain those obtained by Falomo et al. (1991) with a resolution of 0.″7.

With the aim of investigating the close environment of PKS 2155−304, we obtained high-resolution (∼0.″12) NIR images with the innovative Multi-Conjugate Adaptive Optics Demonstrator (MAD) system at the European Southern Observatory (ESO) Very Large Telescope (VLT). In particular, we searched for an NIR counterpart of the radio jet as found with a similar technique in a few other nearby BL Lac objects (PKS 0521−365 and PKS 2201+044; Falomo et al. 2009; Liuzzo et al. 2011a, 2011b). The only other object of this class showing an optical jet is 3C 371 (Scarpa et al. 1999; Sambruna et al. 2007). To complement the new NIR images, we also performed a detailed analysis of archival VLA images and compared them with the new NIR data.

In the following, we adopt the concordance cosmology with $\Omega_m = 0.3$, $\Omega_\lambda = 0.7$, and $H_0 = 70$ km s^{-1} Mpc^{-1}. In this scenario, at $z = 0.116$, 1″corresponds to 2.1 kpc.

2. MAD NEAR-IR DATA

We performed *J*- and *Ks*-band observations (see Figure 1) of PKS 2155−304 on 2007 September 28 using the ESO MAD mounted at UT3 (Melipal) of VLT. MAD is a prototype for the Multi-Conjugate Adaptive optics (MCAO) system that aims to demonstrate the feasibility of different MCAO reconstruction

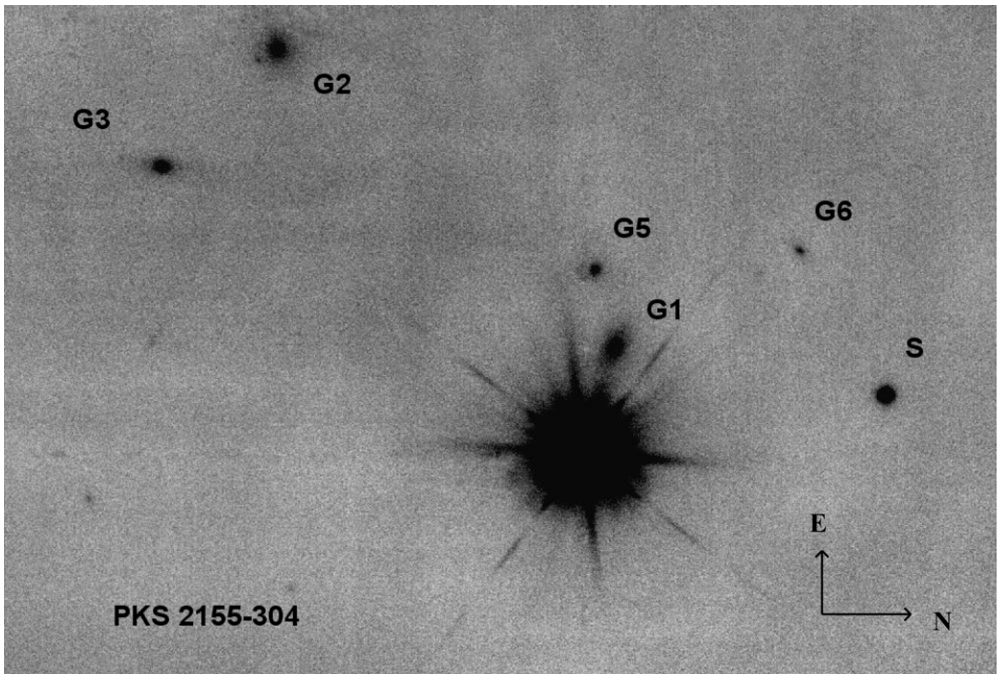

Figure 1. MAD image in the Ks band of the field centered on PKS 2155−304 (the brightest object in the field). The figure covers a ∼30 × 40 arcsec^2 central portion of the observed field. Five galaxies are revealed in the field of the BL Lac object. We name some of them according to Falomo et al. 1993 (see comments in Section 2).

techniques in the framework of the European Extremely Large Telescope concept and the second-generation VLT instruments. MAD is designed to perform wide field-of-view (FoV) adaptive optics correction in J, H, and Ks bands over 2′ on the sky by using relatively bright ($m(V) < 14$–16) Natural Guide Stars. We refer to Marchetti et al. (2003) for a detailed description of MAD. The MCAO correction was obtained using the Layer-Oriented Multi-Pyramid Wave Front Sensor for the MCAO reconstruction (Ragazzoni 1996; Ragazzoni et al. 2000; Marchetti et al. 2005; Arcidiacono et al. 2008). The detector used is a Hawaii-II and it has a 57″ × 57″ FoV with a pixel size of 0.″028.

For these new observations, MAD was configured in the classical single reference approach (also called Single Conjugated Adaptive Optics (SCAO)) since the target is very bright, dominated by the unresolved nucleus, and because in the AO FoV there are no other sufficiently bright stars. This is a different method than that used for previous MAD observations of extragalactic sources (Falomo et al. 2009; Liuzzo et al. 2011a, 2011b). The pyramid wave-front sensor measured an R magnitude of 13 once the adaptive optics loop was closed. The pyramid wave-front sensor measurements corrected the first 35 Zernike modes using the pupil conjugated 60 actuator deformable mirror. PKS 2155−304 was centered on the infrared detector, and a five-position (dice 5) dithering pattern with a 5″ step was applied in order to allow reliable sky subtraction. The dithering pattern was repeated six times for both the J and Ks filters, changing the starting central position of dice 5 three times, in order to reduce the effect of detector artifacts improving the sky background evaluation. The total integration time in each band was 1800 s. The Differential Image Motion Monitor measured a 0.″85 seeing at the zenith in the V band. We obtained 3% and 12% Strehl ratio values in the J and Ks bands, respectively, corresponding to images with a core of 0.″15 and 0.″12 FWHM. In Figure 2, we show the encircled energy distribution derived from the only star in the field (see Figure 1). Half of the total energy is found within $R(50\%)$ ∼0.″13. Due to the faintness of this

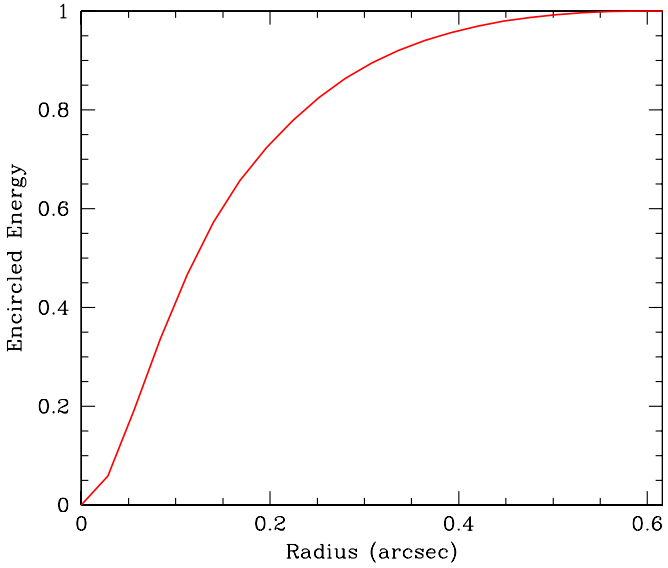

Figure 2. Encircled energy distribution obtained for the only star in the Ks MAD image of PKS 2155−304 (see Figure 1). Fifty percent of the encircled energy is gathered within a radius of 0.″13.

(A color version of this figure is available in the online journal.)

star, no information about the shape of the point-spread function (PSF) is available at radii larger than 0.″8. This prevents us from performing an appropriate modeling of the emission around the target to characterize the host galaxy, which extends up to ∼5″ from the nucleus (Falomo et al. 1991; Kotilainen et al. 1998).

Since the J- and Ks-band images are similar, we show here only images in the Ks band (Figures 1 and 3). A few close-by galaxies are present in the observed field (Figures 1 and 3). Some of them were already detected by Falomo et al. (1991, 1993) and we use their labels for these galaxies (see Table 1). Another companion galaxy (G4) is located ∼2′south of PKS 2155−304

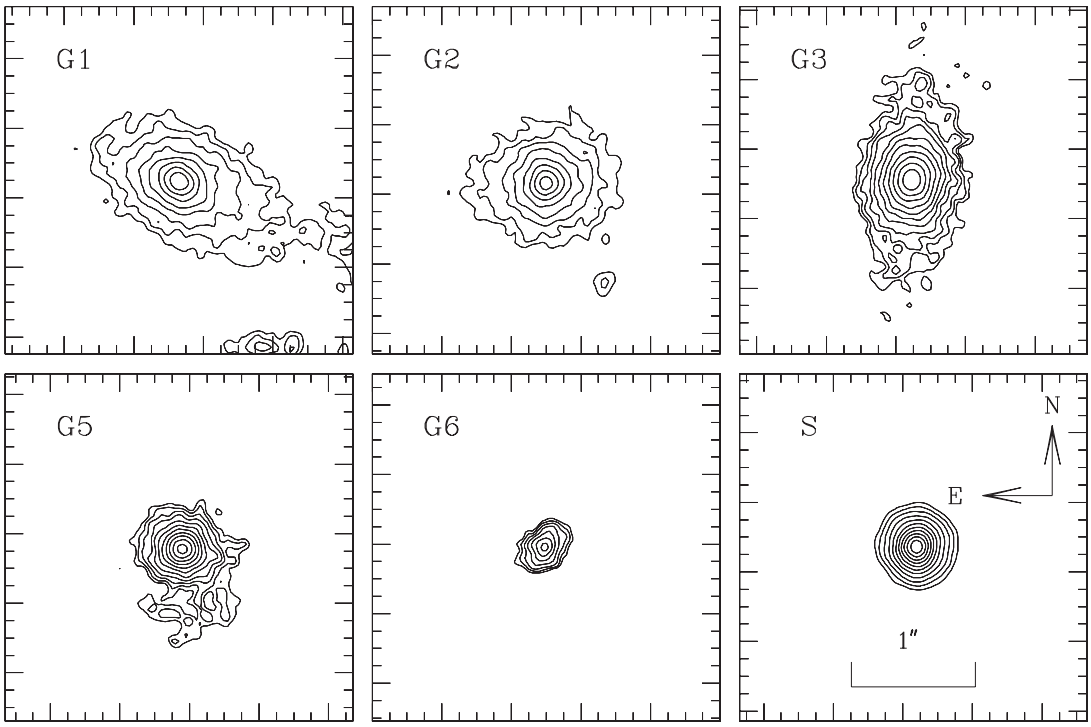

Figure 3. Contour images for the five galaxies plus the only star observed in the field of PKS 2155−304 in our Ks MAD observations.

Table 1
Fundamental Parameters of Five Galaxies in the Field of PKS 2155−304

Galaxy	R.A.(J2000)	Decl.(J2000)	z	Angular Dist. (arcsec)	Notes
G1	21 58 52.385	−30 13 30.52	0.117	4.6	Falomo et al. (1993)
G2	21 58 53.334	−30 13 44.65	···	21.0	Falomo et al. (1993)
G3	21 58 52.958	−30 13 49.47	0.116	21.3	Falomo et al. (1993)
G5	21 58 52.633	−30 13 31.36	···	7.6	This Work
G6	21 58 52.697	−30 13 22.83	···	12.3	This Work

Note. Column 5: angular distance in arcsecond from PKS 2155−304.

Table 2
Basic Data for the Five Galaxies in the Field of PKS 2155−304

Galaxy	Ks	J	$R_{\rm eff}$ (arcsec)	e
G1	16.1	16.9	0.78	0.5
G2	16.1	17.0	0.65	0.1
G3	16.9	18.1	0.30	0.5
G5	17.7	18.5	0.65	0.2
G6	19.5	19.4	0.62	0.6

Notes. Magnitudes are obtained with a precision of ∼0.1 mag.
Column 4: $R_{\rm eff}$ is the effective radius from the Ks band.
Column 5: e indicates source ellipticity.

(out of the FoV of our MAD images). This is a bright galaxy ($R = 16.5$) at the same redshift of the BL Lac object (Falomo et al. 1993). J- and Ks-band properties of the five galaxies are reported in Table 2. G1 and G3 are at the same redshift as PKS 2155−304 (see Table 1). For the other galaxies, no spectroscopy is available. Assuming these galaxies to be at the same distance to the BL Lac object and a standard $H-K$ color, they could represent low-luminosity (absolute magnitude in the H-band M_H in the range [−22.4;−19.0] versus $M_H = -26.8$ for PKS 2155−304; Kotilainen et al. 1998) and small ($R_{\rm eff}$ ∼1.5 kpc) satellite galaxies.

Table 3
Parameters of Multifrequency Radio Images

Data (yy/mm/dd)	ν (GHz)	HPBW ($'' \times ''$,°)	rms (mJy beam^{-1})	$F_{\rm peak}$ (Jy beam^{-1})	$F_{\rm tot}$ (Jy)
94/05/14	1.4 (L)	5.7 × 3.1, 44	0.3	0.38	0.41
94/05/14	4.8 (C)	3.0 × 3.0, 0	0.1	0.42	0.44
94/05/14	8.4 (X)	1.1 × 0.7, 20	0.2	0.43	0.44
94/05/14	15 (U)	0.5 × 0.4, 82	0.2	0.44	0.45
94/05/14	22.5 (K)	0.2 × 0.2, 47	0.8	0.40	0.40
03/07/24	8.4 (X)	0.6 × 0.2, −22	0.1	0.21	0.22

Notes. Column 1: observing data.
Column 2: observing frequency.
Column 3: HPBW (half-power beam width) and position angle of the major axis in degrees.
Column 4: 1 rms level.
Column 5: peak flux density.
Column 6: total flux density.

3. RADIO DATA

To characterize the arcsecond morphology of PKS 2155−304, we retrieved from the National Radio Astronomy Observatory archive VLA radio observations at different frequencies with resolution comparable to that of our NIR MAD images. We

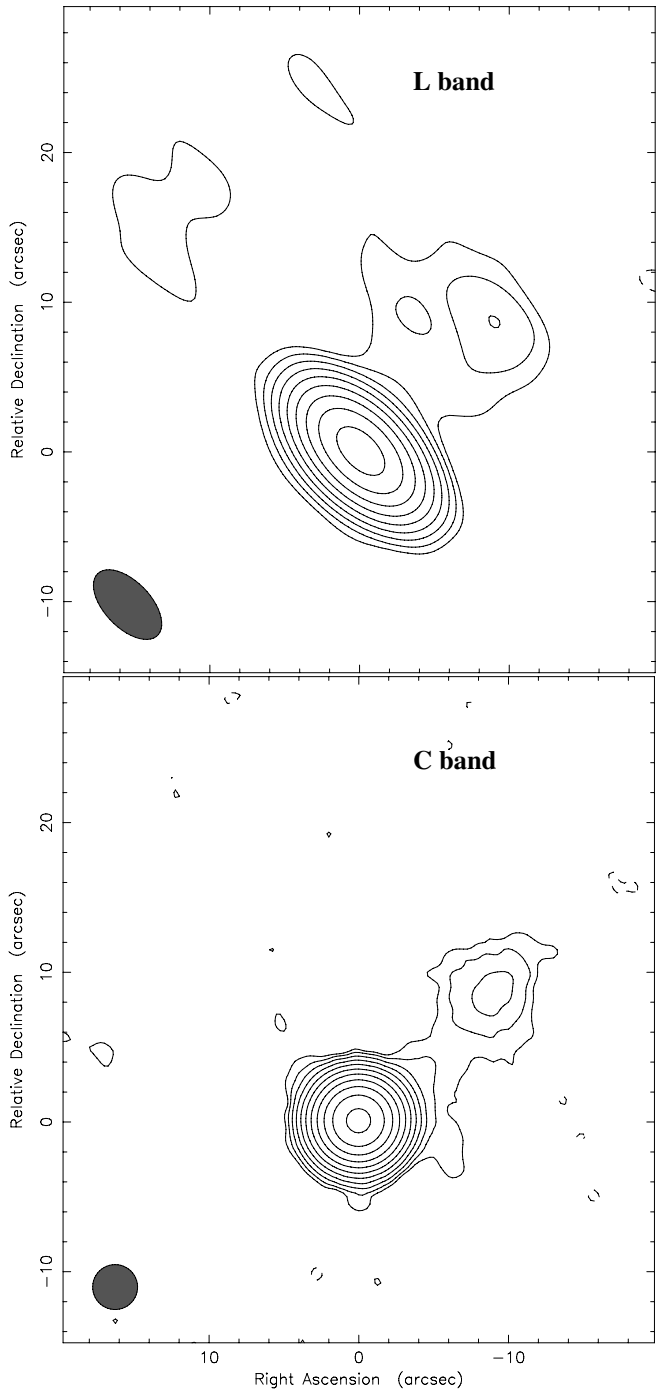

Figure 4. VLA radio contour images of PKS 2155−304 in the *L* band (top panel) and the *C* band (bottom panel). Noise levels, peak, and total flux densities are reported in Table 3. Contour levels are 1 × (1.1, 2.2, 4, 4.4, 8.8, 17.6, 35.2, 70.4, 140.8, and 281.6) mJy beam^{-1} for the *L* band and 0.4 × (1, 2, 4, 8, 16, 32, 64, 128, 258, 516, and 1032) mJy beam^{-1} for the *C* band. North is to the top and east to the left.

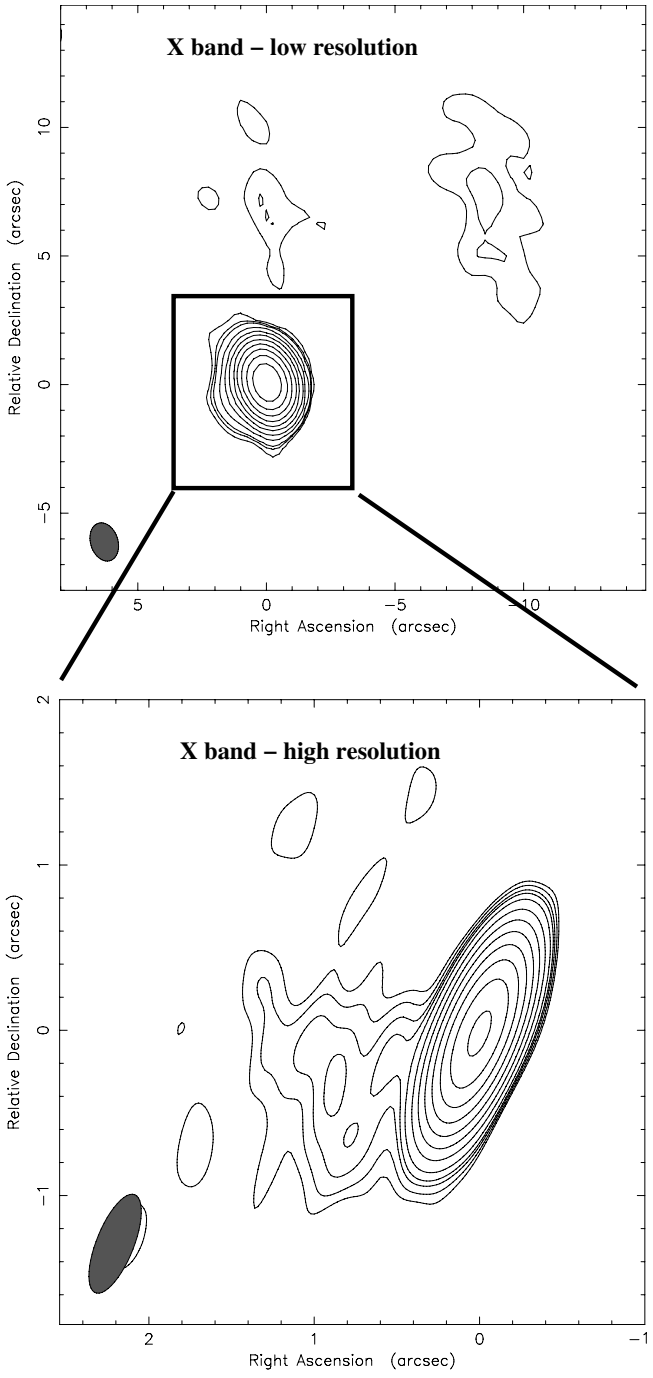

Figure 5. *X*-band low-resolution (top) and high-resolution (bottom) VLA radio contour images of the central region (rectangle in the top panel) of PKS 2155−304. Noise levels, peak, and total flux densities are reported in Table 3. Contour levels are 0.38 ×(1.06, 1.6, 3.2, 6.4, 12.8, 25.6, 51.2, 102.4, 204.8, and 409.6 for *X*-band low resolution and 0.36 × (1.06, 1.6, 2.3, 2.8, 3.2, 6.4, 12.8, 25.6, 51.2, 102.4, 204.8, 409.6, and 819.2) mJy beam^{-1} for *X*-band high resolution. North is to the top and east to the left.

analyzed simultaneous data obtained in *L* (1.4 GHz), *C* (5 GHz), *X* (8.4 GHz), *U* (15 GHz), and *K* (22.5 GHz) bands with the VLA BnA configuration on 1994 May 14 (Project ID AK0359), and one observation in the *X* band with the VLA A configuration taken on 2003 July 24 (Project ID AR0517).

The target was observed for ∼6.5 minutes at 1.4 and 4.8 GHz, while the 8.4, 15, and 22.5 GHz observations have a total time on source of ∼40 minutes. To produce our final images, we calibrated the data with the standard procedures in the Astronomical Information Processing System, accurately edited the visibilities, and carried out a few self-calibration cycles. The final images are produced with the IMAGR task. Image parameters are given in Table 3. Typical errors for flux measurements are ∼3% for frequencies lower than 8.4 GHz and ∼10% for higher ones. In Figures 4 and 5, we present the most significant (*L*, *C*, and *X* bands) among our analyzed multifrequency VLA images. In particular, maps in Figure 4 and in the top panel of

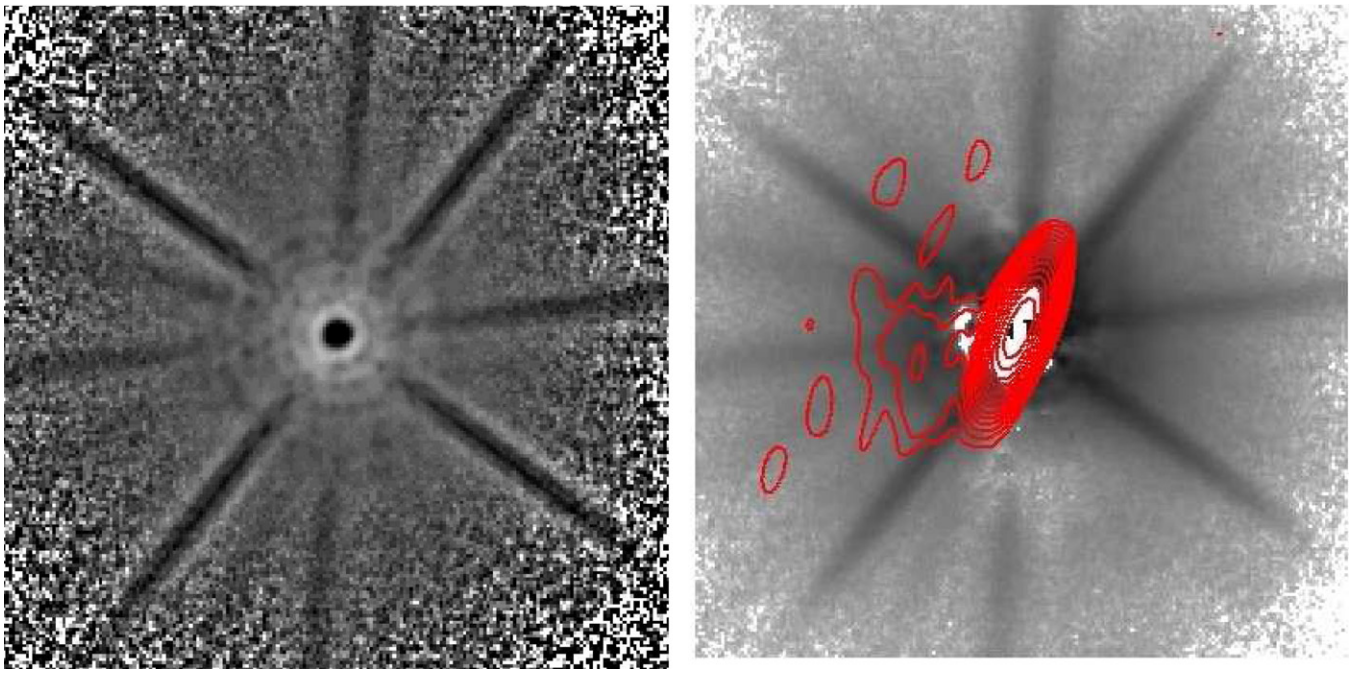

Figure 6. Left: image of PKS 2155−304 obtained using unsharp masking to enhance the high-contrast features. The diffraction pattern due to the VLT secondary mirror and by the pupil mask of the ground conjugated deformable mirror (the sharp one) are the most prominent components of the PSF. The inner region shows in the residual a ring pattern that follows both in ring intensity and radii the diffraction-limited PSF profile in the Ks band. The spotty structure over the rings is common in adaptive-optics-corrected images: the diffraction patterns are modulated in intensity, creating speckles. Right: contour image VLA map in *X*-band low-resolution imaging of PKS 2155−304 overimposed on the grayscale MAD image after the subtraction of a scaled PSF defined by the only star in the field of the BL Lac object (see also Figure 1).

(A color version of this figure is available in the online journal.)

Figure 5 are taken from the 1994 data, while the *X*-band high resolution (Figure 5, bottom panel) is obtained from 2003 observations. Comparing the total flux densities at the two epochs (1994 and 2003, Table 3), PKS 2155−304 shows clear evidence of variability in its non-thermal continuum emission, which is a common feature for BL Lac objects (Urry & Padovani 1995) and is consistent with previous observations (e.g., Kedziora-Chudczer et al. 2001).

Concerning the morphology, at low resolution (*L* band, Figure 4, top panel), PKS 2155−304 is dominated by a bright core with a peak flux density of 0.38 Jy beam^{-1} and a second component is present at 12″ from the core in the NW direction with a flux density of ∼0.3 Jy. We also made a tapered image where an eastern diffuse emission is barely visible corresponding to the EW structure found by Ulvestad & Antonucci (1986). A core plus the NW knot are also revealed in our *C*-band data (Figure 4, bottom panel). At intermediate frequency (*X* band, ∼0.″7 resolution), the NW component observed at lower frequencies is dimly visible only in tapered images of the 1994 epoch (Figure 5, top panel), where the eastern jet is slightly resolved. However, in the 2003 maps (∼0.″2), the eastern jet clearly appears with an extension of ∼1″from the nucleus and a total flux density of ∼0.01 Jy (Figure 5, bottom panel).

At higher frequency (*U* band, ∼0.″5 resolution), the jet component is resolved with an angular dimension of ∼2″ and a flux density of ∼0.01 Jy, and it is oriented in the same direction of the mass structure found, e.g., by Piner et al. (2010). Finally, in the *K*-band map (∼0.″2 resolution), the source is unresolved (peak flux density of ∼0.4 Jy beam^{-1}) and the jet is undetected up to 3.2 mJy beam^{-1}.

The eastern jet is also revealed in our analysis of archival Very Long Baseline Array *L*-band data of 2000 January 15 with a final resolution of ∼14 mas, which is intermediate between VLBI- and VLA-published images up to now (∼1 mas and ∼0.″5 resolution, respectively). The structure is aligned with the sub-kpc jet (Figure 6 and Ulvestad & Antonucci 1986; Laurent-Muehleisen et al. 1993). From this alignment, one could argue that black hole precession does not occur between these two angular scales.

In order to further investigate the nature of the source components, we made spectral index maps from the simultaneous multiwavelength data taken in 1994. For all of the maps that we produced, we used data closest in frequency and constructed with the same angular resolution. We define spectral index α as $S \sim \nu^{\alpha}$, where S is the flux density at frequency ν. At the arcsecond scale, the NW knot shows a steep spectral index (∼(−0.5)) that we interpreted as being due to old radio emission. At the sub-arcsecond scale, the spectral indices of the eastern jet vary radially from 0 to −1 according to the typical radiative and adiabatic losses of jets. At all resolutions, the central (0.″5) region has a flat spectral index, while outside, the α distribution is more complex, with some asymmetries in the transverse direction, suggesting the presence of large-scale helical magnetic field structure (cf. Clausen-Brown et al. 2011).

4. COMPARISON OF RADIO AND NIR IMAGES

We searched for radio emission associated with the five close-by galaxies in the field of PKS 2155−304 (see Figure 1 and Table 1) using VLA archival data. No radio counterparts were found above the 1 mJy level.

In order to investigate the presence of the NIR counterpart of the eastern radio jet, in Figure 6, we show the comparison between the MAD NIR image with the *X*-band high-resolution

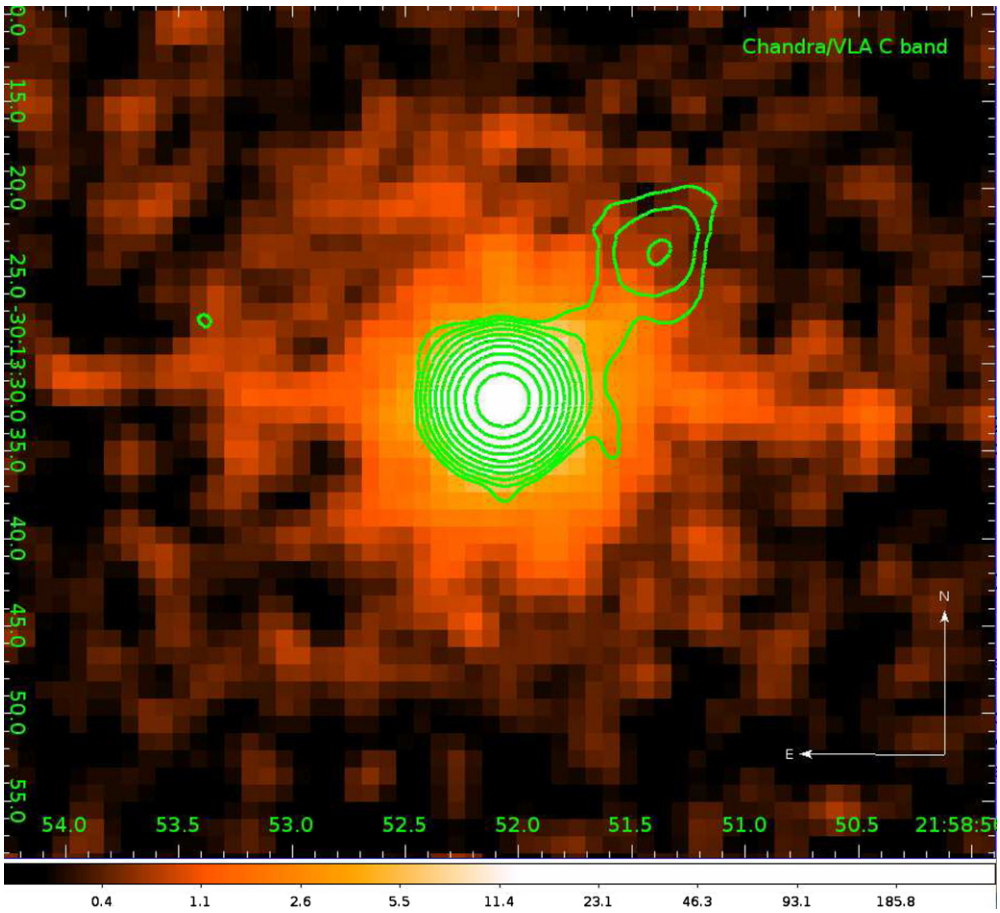

Figure 7. *Chandra*/HETG image of PKS 2155−304 with a VLA *C*-band contour map overimposed. The X-ray observation was taken on 2008 July 2 for a total exposure of ∼15 ks. The X-ray image in the 0.4–8 keV range was extracted from the Transmission Grating and Catalog archive (TGCat archive (http://tgcat.mit.edu/); Huenemoerder et al. 2011). The image was then smoothed with a Gaussian function of kernel radius 2.

(A color version of this figure is available in the online journal.)

radio map (see also Figure 5). The MAD map is obtained by subtracting a scaled point source modeled by the north faint star at ∼12.″7 (see Figure 1). Due to the faintness of this star, it is possible to define the PSF model only up to 0.″8 from the center (Section 2 does not account for the prominent diffraction figure of the PSF). At larger angular distance, we therefore used an extrapolation of the model. In Figure 6, we show the complex structure of the PSF and the result of the subtraction of the model for the core of the PSF.

In our MAD images, there is no counterpart in the NIR band of the eastern radio jet up to a magnitude limit of $m_K = 16.5$; whereas, in our previous studies of NIR counterparts of radio jets in BL Lac objects, we observed the brightest radio knot in PKS 0521−365 (Falomo et al. 2009) at a distance from the core (d) ∼2″and $m_K = 17.6$, and in PKS 2201+044 (Liuzzo et al. 2011b) at d ∼2.″2 and $m_K = 18.5$. Finally, we also investigated the morphology of PKS 2155−304 in the X-ray band. The *Chandra* X-ray satellite is the ideal instrument for this aim since it allows us to perform spatially resolved studies thanks to its unprecedented angular resolution (PSF FWHM 0.″5). Figure 7 shows a *Chandra*/HETG archival image with a VLA *C*-band contour map overimposed. We found no possible evident structures associated with the radio jet.

This work was supported by contributions from the European Union, the Valle D'Aosta Region, and the Italian Ministry for Work and Welfare. This research has made use of the NASA/IPAC Extragalactic Data Base (NED), which is operated by the JPL, California Institute of Technology, under contract with the National Aeronautics and Space Administration.

REFERENCES

Aharonian, F., Akhperjanian, A. G., Anton, G., et al. 2009, ApJL, 696, L150
Aharonian, F., Akhperjanian, A. G., Bazer-Bachi, A. R., et al. 2005, A&A, 442, 895
Aharonian, F., Akhperjanian, A. G., Bazer-Bachi, A. R., et al. 2007, ApJL, 664, L71
Arcidiacono, C., Lombini, M., Ragazzoni, R., et al. 2008, Proc. SPIE, 7015, 70155P
Clausen-Brown, E., Lyutikov, M., & Kharb, P. 2011, MNRAS, 415, 2081
Falomo, R., Giraud, E., Melnick, J., et al. 1991, ApJL, 380, L67
Falomo, R., Pesce, J. E., & Treves, A. 1993, ApJL, 411, L63
Falomo, R., Pian, E., Treves, A., et al. 2009, A&A, 501, 907
Foschini, L., Ghisellini, G., Tavecchio, F., et al. 2007, ApJL, 657, L81
Foschini, L., Treves, A., Tavecchio, F., et al. 2008, A&A, 484, L35
Huenemoerder, D. P., Mitschang, A., Dewey, D., et al. 2011, AJ, 141, 129
Kedziora-Chudczer, L. L., Jauncey, D. L., Wieringa, M. H., Tzioumis, A. K., & Reynolds, J. E. 2001, MNRAS, 325, 1411
Kotilainen, J. K., Falomo, R., & Scarpa, R. 1998, A&A, 336, 479
Laurent-Muehleisen, S. A., Kollgaard, R. I., Moellenbrock, G. A., & Feigelson, E. D. 1993, AJ, 106, 875
Liuzzo, E., Falomo, R., & Treves, A. 2011a, in Proceedings of Science, vol. 126, The Properties of Nearby BL Lac Objects with Optical Jets, ed. L. Foschini, M. Colpi, L. Gallo et al. (PoS(NLS1)058) http://pos.sissa.it/cgi-bin/reader/conf.cgi?confid=126
Liuzzo, E., Falomo, R., Treves, A., et al. 2011b, A&A, 528, A34

Marchetti, E., Brast, R., Delabre, B., et al. 2005, CRPhy, 6, 1118
Marchetti, E., Hubin, N. N., Fedrigo, E., et al. 2003, Proc. SPIE, 4839, 317
Marshall, H. L., Urry, C. M., Sambruna, R. M., & Pesce, J. E. 2001, ApJ, 549, 938
Ojha, R., Fey, A. L., Johnston, K. J., et al. 2004, AJ, 127, 3609
Ojha, R., Kadler, M., Böck, M., et al. 2010, A&A, 519, A45
Piner, B. G., & Edwards, P. G. 2004, ApJ, 600, 115
Piner, B. G., Pant, N., & Edwards, P. G. 2008, ApJ, 678, 64
Piner, B. G., Pant, N., & Edwards, P. G. 2010, ApJ, 723, 1150
Ragazzoni, R. 1996, JMOp, 43, 289
Ragazzoni, R., Farinato, J., & Marchetti, E. 2000, Proc. SPIE, 4007, 1076
Sakamoto, Y., Nishijima, K., Mizukami, T., et al. 2008, ApJ, 676, 113
Sambruna, R. M., Donato, D., Tavecchio, F., et al. 2007, ApJ, 670, 74
Sbarufatti, B., Falomo, R., Treves, A., & Kotilainen, J. 2006, A&A, 457, 35
Scarpa, R., Urry, C. M., Falomo, R., Pesce, J. E., & Treves, A. 2000, ApJ, 532, 740
Scarpa, R., Urry, C. M., Falomo, R., & Treves, A. 1999, ApJ, 526, 643
Ulvestad, J. S., & Antonucci, R. R. J. 1986, AJ, 92, 6
Urry, C. M., Maraschi, L., Edelson, R., et al. 1993, ApJ, 411, 614
Urry, C. M., & Padovani, P. 1995, PASP, 107, 803
Urry, C. M., Treves, A., Maraschi, L., et al. 1997, ApJ, 486, 799